A *Ku*-Band Oscillator Utilizing Overtone Lithium Niobate RF-MEMS Resonator for 5G

Ali Kourani, *Graduate Student Member, IEEE*, Yansong Yang, *Member, IEEE*, and Songbin Gong, *Senior Member, IEEE*

***Abstract*— This letter presents a 12.9-GHz silicon germanium (SiGe) Pierce oscillator using a third antisymmetric overtone in a lithium niobate ($LiNbO_3$) resonator for 5G communications. Quarter-wave resonators are used to satisfy the Barkhausen oscillation conditions for the third overtone while suppressing the fundamental and higher order resonances. The oscillator achieves a measured phase noise of −70 and −111 dBc/Hz at 1 and 100-kHz offsets from a 12.9-GHz carrier while consuming 20 mW of dc power. The oscillator achieves a figure-of-merit of 200 dBc/Hz at 100-kHz offset, surpassing the state-of-the-art electromagnetic (EM) and overtone MEMS oscillators. The achieved oscillation frequency is the highest reported to date for an MEMS oscillator. The demonstrated performance shows the strong potential of microwave acoustic oscillators for 5G frequency synthesis. This work will enable low-power 5G transceivers featuring high speed, high sensitivity, and high selectivity in small form factors.**

***Index Terms*— Lithium niobate ($LiNbO_3$), MEMS, oscillator, overtone.**

I. Introduction

CURRENTLY, the sub-3-GHz frequency bands are too congested to meet the ever-increasing data rates and communication speeds demanded by many cellular users. The call for higher bandwidths and speeds has pushed the 5G radios toward millimeter (mm)-wave frequencies such as 26–28 and 37–43.5 GHz. Apart from larger bandwidth, 5G wireless transceivers are expected to feature higher sensitivity and selectivity while producing longer battery life; all in small form factors.

To achieve all the above seamlessly, the heartbeat of the transceiver—namely, the frequency synthesizer—must be revolutionized on architecture, circuit, and device levels. Local oscillator (LO) noise directly adds to the transceiver noise figure (NF) and worsens the sensitivity while any spurs on LO considerably exacerbate the selectivity. To relax the requirements on the sensitivity and selectivity of the RF front-end for 5G, the synthesizer phase noise has to be reduced through a nonconventional way. One key challenge in implementing high-performance chip-scale synthesizers for 5G beyond 10 GHz lies in the lack of high-performance miniature resonators that can enable signal generation with minimal phase noise and power consumption.

The state-of-the-art (SoA) microwave oscillators are based on *LC* [1], microstrip [2], active [3], and dielectric resonators (DRs) [4]. On-chip lossy *LC* tanks are compact, hence offering a low-cost solution. However, their low Q at microwave frequencies translates to poor phase noise and high-power consumption. Quarter wavelength electromagnetic (EM) resonators have footprints on the order of 7.5 mm for a 10-GHz resonance, making them too bulky for handsets. DROs offer superior phase noise performance, but they are bulky and consume a large amount of power.

Alternatively, oscillators based on RF-MEMS resonators that harness the confinement of acoustic waves and have the size of hundreds of microns are attractive for portable devices. Recently, acoustic resonators with resonances above 10 GHz have been demonstrated in different platforms such as aluminum nitride (AlN) thin-film bulk acoustic resonators (FBARs) [5], AlN contour mode resonators (CMRs) [6], [7], scandium-doped AlN resonators [8], [9], ferroelectric resonators [10], FinFET resonators [11], and lithium niobate ($LiNbO_3$) resonators [12]–[14]. From this group, $LiNbO_3$ resonators feature the highest demonstrated figure-of-merit ($FoM_{RES} = Q \times$ electromechanical coupling coefficient, k_t^2) making them the more suitable candidate for enabling chip-scale oscillators with simultaneously low phase noise and low power consumption [15], [16].

To this end, this letter reports on the first acoustic microwave oscillator based on $LiNbO_3$ RF-MEMS resonators. A *Ku*-band Pierce oscillator using a third overtone $LiNbO_3$ resonator is presented. The oscillator is demonstrated with a phase noise of −70 and −111 dBc/Hz at 1 and 100-kHz offsets from a 12.9-GHz carrier, harnessing a third overtone characterized by a loaded quality factor (Q_l) of 270, k_t^2 of 1.9%, and an FOM_{RES} of 5.1. The oscillator consumes a dc power of 20 mW achieving an FoM_{OSC} of 200 dBc/Hz at 100-kHz offset. The demonstrated performance shows the strong potential of acoustic microwave oscillators to revolutionize the 5G frequency synthesis. Their main strength lies in offering small form factor and long battery life solutions with competitive phase noise results compared with other EM oscillators.

II. Oscillator Design

A. Antisymmetric Mode $LiNbO_3$ RF-MEMS Resonators

Antisymmetric modes are a class of Lamb-wave modes characterized by their antisymmetric vibrations about the median plane of the plate. These modes have equal vertical but opposite longitudinal displacement components on the opposite sides of the median plane. The theory defining the resonant frequencies for the excited odd modes can be found in [12]. The higher order antisymmetric modes are confined in the unmetallized regions between any two electrodes. Such confinement is a result of the acoustic impedance mismatch between the metalized and unmetalized sections. Hence, half

Manuscript received March 14, 2020; revised April 25, 2020; accepted May 11, 2020. Date of publication June 2, 2020; date of current version July 7, 2020. *(Corresponding author: Ali Kourani.)*

The authors are with the Department of Electrical and Computer Engineering, University of Illinois at Urbana–Champaign, Urbana, IL 61801-3028 USA (e-mail: kourani2@illinois.edu).

Color versions of one or more of the figures in this letter are available online at http://ieeexplore.ieee.org.

Digital Object Identifier 10.1109/LMWC.2020.2996961

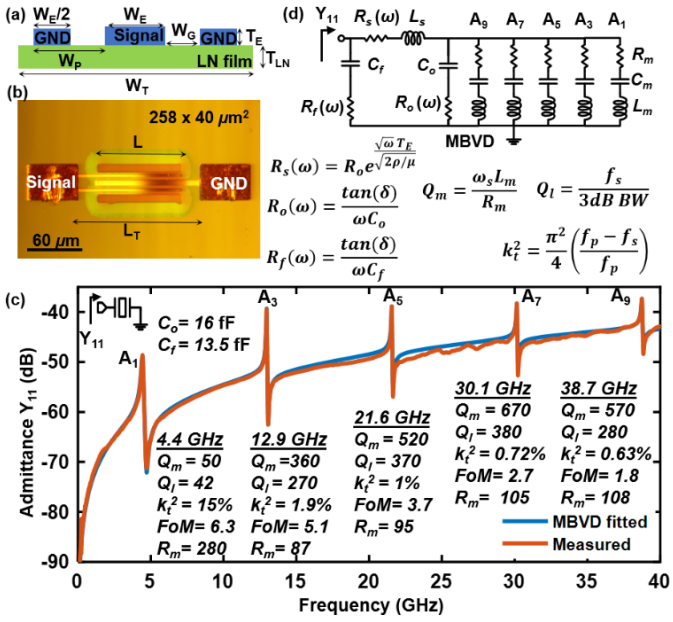

Fig. 1. (a) Mockup cross-sectional view of the $LiNbO_3$ resonator with key parameters is shown. $W_T = 21\ \mu$m, $W_G = W_E/2 = 3\ \mu$m, $T_E = 50$ nm, the thickness of the electroplated Au pad is 2 μm, $T_{LN} = 400$ nm, $L_T = 142\ \mu$m, $L = 100\ \mu$m, and the pad area is $60 \times 40\ \mu m^2$. (b) Optical image of the fabricated resonator. (c) Measured and MBVD fit response for the first five odd modes. (d) Multiresonance equivalent MBVD model with parasitics included. $\tan(\delta)$ is the loss tangent of $LiNbO_3$, ρ is the resistivity of thin-film Au, and μ is the permeability of Au. Mechanical (Q_m), loaded (Q_l) quality factors, k_t^2, FoM, and R_m of each tone are shown.

the longitudinal wavelength ($\lambda_l/2$) is approximately equal to the distance between the adjacent electrodes (W_G). The resonance of an A-mode resonator is largely set by the thickness of the $LiNbO_3$ film (T_{LN}) and the mode order (m). Hence, for a resonator using a 400-nm-thick Z-cut $LiNbO_3$ film, $\lambda_l = 6\ \mu$m, and m of 3, the A_3 resonance rises beyond 10 GHz which is desired for investigating microwave acoustic oscillators.

The resonator comprised a three-electrode transducer on the top of a mechanically suspended Z-cut $LiNbO_3$ thin film as shown in Fig. 1(a) and (b). The electrodes being connected to signal and ground induce lateral electric fields in the piezoelectric film, hence exciting the resonator into odd-order antisymmetric vibrations. The resonator was fabricated, with the dimensions given in the inset of Fig. 1, using a process described in [17]. A 50-nm gold (Au) is sputtered and lifted-off as top electrodes. Au probing pads of $60 \times 40\ \mu m^2$ are electroplated to 2-μm thickness with a 200-μm pitch to reduce the parasitics between the pads.

The resonator was measured and characterized using the Keysight N5230A PNA-L network analyzer. A thru-reflect-line (TRL) calibration is done in measurements using on-wafer standards. A multiresonance modified Butterworth–Van Dyke (MBVD) model shown in Fig. 1(d) is used to interpret the measured admittance shown in Fig. 1(c). The MBVD model includes an additional series inductor ($L_s = 90$ pH) and a resistor ($R_s = 13.4\ \Omega$ at 13 GHz) to model the nonnegligible inductance and the surface resistance of the electrodes at high frequencies, respectively. It also includes a capacitor of 13.5 fF and a resistor (R_f) to model the feedthrough capacitance (C_f), and the resistive substrate loss, respectively. The resonator is also characterized by a static capacitance from the IDT (C_o)

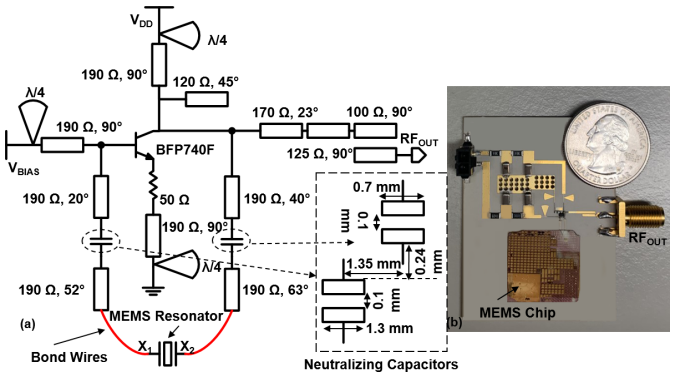

Fig. 2. (a) Simplified schematic of the RF portion of the 13-GHz oscillator. (b) Oscillator PCB.

of 16 fF, which is set by the size of the resonator. The loaded quality factor (Q_l) is measured for each resonance using the 3-dB bandwidth method, while the mechanical quality factor (Q_m) is extracted through the MBVD model by excluding the electrical loss. k_t^2 is also extracted for each resonance considering all the device parasitics.

The first five odd modes, A_1, A_3, A_5, A_7, and A_9, with resonances at 4.4, 13, 22, 30, and 39 GHz are characterized. The key measured and extracted parameters, including Q_l, Q_m, and k_t^2, are shown in Fig. 1(c). For higher order modes, Q_l is 270 for A_3 and 380 for A_7, while Q_m is 360 for A_3, and 670 for A_7. For these modes, Q_m varies from 1.3 Q_l at 13 GHz to $2Q_l$ at 39 GHz, indicating that mitigating electrical loss is crucial for high performance at microwave and mm-wave frequencies. k_t^2 decreases from 15% for A_1 to 0.63% for A_9 with a value of 1.9% for A_3. The reason behind the degradation of k_t^2 with an increasing mode order can be found in [12].

Optimizing the resonator for higher FoM_{RES} is desirable to enable oscillations with low-power consumption and good phase noise metrics. This can be achieved through improving the thin-film quality, using metals with lower mechanical losses for IDEs, and using SiC or sapphire as a substrate to reduce the dielectric loss.

B. Pierce Oscillator

The Pierce oscillator shown in Fig. 2(a) is used to excite the resonator third overtone at 13 GHz. Infineon BFP740F silicon germanium (SiGe) n-p-n heterojunction bipolar transistor (HBT) is used for its low NF which is critical for low phase noise oscillations. The transistor has cut-off frequencies f_t of approximately 45 and 27 GHz at collector currents I_C of 25 and 5 mA. Rather than any higher order resonance, A_3 is chosen for a low-power solution primarily due to the limitations of f_t. Bias voltages V_{CE} and V_{BE} of 2.7 and 0.8 V, respectively, are chosen for optimal phase noise performance while consuming 20 mW of dc power. A 50-Ω degeneration resistor is used to set the transistor bias and help in boosting the linearity at the expense of slightly higher power consumption.

The resonator-loading reactances needed for the Pierce operation at 13 GHz are realized mainly through the transistor junction capacitances (C_{CB} of 80 fF, C_{CE} of 0.3 pF, and C_{BE} of 0.4 pF) and an open circuit stub of 120 Ω and 45° in electrical length at 13 GHz. The stub creates a reactance equivalent to a capacitance of 100 fF at the collector terminal. In addition, the resonator static capacitance C_o, the feedthrough

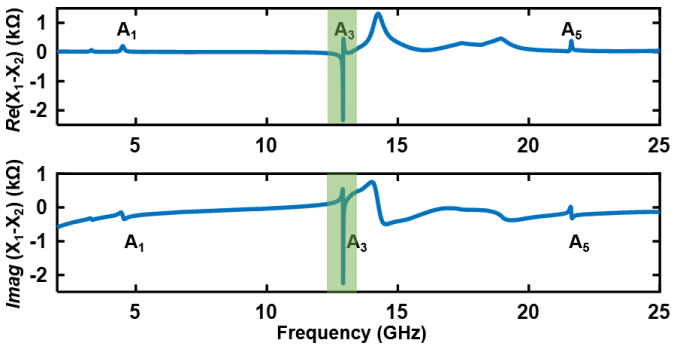

Fig. 3. Simulated real and imaginary input impedances across circuit nodes X_1 and X_2. Only the third-order mode is excited.

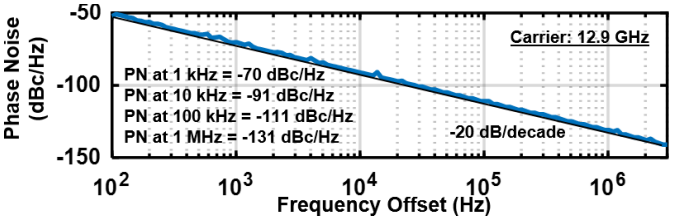

Fig. 4. Measured phase noise of the 13-GHz carrier.

capacitance C_f, and the printed circuit board (PCB) parasitic capacitances are also included in the loading reactance.

Bias-Tees are critical in the design for optimal performance. Open $\lambda/4$ radial stub of low impedance is used to create an RF choke in the dc arm, hence allowing the dc bias and isolating RF from the bias network [not shown in Fig. 2(a)]. A high-impedance (190 Ω) $\lambda/4$ line is used to transform the RF short to an RF open circuit at all the transistor terminals. Thus, the biasing arm does not load the RF path. The lengths of the quarter-wave stubs are chosen for 13 GHz. An output matching network is used for 50-Ω measurements. The network is designed to have a low insertion loss for high output power and low noise floor, while not loading the collector or worsen the flicker and thermal phase noises.

To satisfy the Barkhausen's loop-phase condition of oscillation, special attention is given to the trace between the base and the collector. Hence, the transmission lines' impedances, lengths, and the resonator wire bonds are extensively simulated using Keysight Momentum. Variations in the trace lengths will change the frequency of oscillation and the phase noise profile. Two capacitors in the positive feedback path are implemented as parallel traces to neutralize the wire bonds' inductances, and hence force the frequency of oscillation to be as close to A_3 resonance as possible, thus enhancing the loaded Q and the phase noise. The oscillator is assembled on a Rogers RO3003 board with a thickness of 1.52 mm, a dielectric constant of 3, and a dissipation factor of 0.0013 at 10 GHz. The conditions of oscillation are satisfied for only the third-order resonance, while the fundamental and higher order resonances are suppressed as shown in Fig. 3.

III. Measurements

The active portion of the Pierce oscillator on the Rogers RO3003 board is integrated with the MEMS chip (2 cm×2 cm) through wire bonding. The assembly is shown in Fig. 2(b). Phase noise measurements are taken using an R&S FSUP26 signal analyzer and reported in Fig. 4. The oscillator achieves a measured phase noise of −70 and −111 dBc/Hz at 1 and 100-kHz offsets from a 12.9-GHz carrier. The phase noise profile shows a −20 dB/decade trend between 100 Hz and 1 MHz offsets from the carrier. The −30 dB/decade trend is not captured in the region of interest due to the low flicker noise characteristics of the SiGe transistor. For the reported phase noise values, the oscillator consumes a dc power of 20 mW and achieves an FoM_{OSC} of 200 dBc/Hz at 100-kHz offset. The measured output power is −8.5 dBm.

TABLE I
Comparison to the SoA RF-MEMS Oscillators Above 5 GHz

		This work	[18]		[19]	[20]	
Resonator		**$LiNbO_3$ 3rd tone**	FBAR fundamental		FBAR fundamental	FBAR 3rd tone	
IC Process		**discrete**	0.35 μm BiCMOS		discrete	discrete	
Osc. Freq. (GHz)		**12.9**	5.46		5	7	
Resonator footprint (mm^2)		**0.01**	0.034		> 0.1	-	
Q_l		**270**	300#		300	1350	
k_t^2 (%)		**1.9**	6.67#		4.3	-	
FoM_{RES}		**5.1**	20		12.9	-	
dc power (mW)		**20**	12.7		-	16.2	
PN (dBc/Hz)	1 kHz	**-70**	-64^	-56.5	-	-	
	100 kHz	**-111**	-117.7	-110.2	-109.5	-101	-80 -74.7
	1 MHz	**-131**	-		-	-110	-104.7
FoM_{Osc} (dBc/Hz)	100 kHz	**200.2**	201.4		-	164.8	

TABLE II
Comparison to the SoA EM Oscillators

		This work	[4]			[2]	[3]	[1]
Resonator		**$LiNbO_3$**	DRO			µstrip	Active	LC
IC Process		**discrete**	GaN	GaAs	SiGe	BJT	discrete	BiCMOS
Osc. Freq. (GHz)		**12.9**	10.6			10	10	15
Resonator footprint (mm^2)		**0.01**	-			-	-	-
Q_l		**270**	600			-	1211	-
dc power (mW)		**20**	-			200	500	72
PN (dBc/Hz)	1 kHz	**-70**	-53ǂ	-76ǂ	-90ǂ	-65†	-	-
			-51.3	-74.3	-88.3	-62.8		
	100 kHz	**-111**	-118	-123	-135	-113	-114.4	-102*
			-116.3	-121.3	-133.3	-110.8	-112.2	-103.3
FoM_{Osc} (dBc/Hz)	100 kHz	**200.2**	-			190	187.4	187

The values in the shaded cells are referenced to a 12.9 GHz output. # as reported in [21]. ^ value estimated from a plot in [18]. ǂǂ value estimated from a plot in [4]. † value estimated from a plot in [2]. *value estimated from a plot in [1]. $FoM_{OSC} = -L(\Delta f) + 20\log\left(\frac{f_o}{f_m}\right) - 10\log\left(\frac{P_{dc}}{1\,mW}\right)$, where $L(\Delta f)$ is the phase noise measured at an offset f_m from a carrier f_o, and P_{dc} is the dc power consumption.

IV. Conclusion

In comparison to the SoA in Tables I and II, the FoM of our oscillator surpasses those of the SoA EM and overtone MEMS oscillators. Moreover, the achieved oscillation frequency is the highest reported to date for an RF-MEMS oscillator. The demonstrated performance shows the strong potential of microwave acoustic oscillators for 5G frequency synthesis. They offer small form factors and long battery life solutions with competitive phase noise performance in comparison to other EM oscillators. Further reduction in footprint and power consumption can be achieved by realizing the active circuit with a recent CMOS node.

REFERENCES

[1] F. Padovan, F. Quadrelli, M. Bassi, M. Tiebout, and A. Bevilacqua, "A quad-core 15 GHz BiCMOS VCO with −124dBc/Hz phase noise at 1 MHz offset, −189dBc/Hz FOM, and robust to multimode concurrent oscillations," in *IEEE Int. Solid-State Circuits Conf. (ISSCC) Dig. Tech. Papers*, Feb. 2018, pp. 376–377.

[2] A. Khanna, E. Topacio, E. Gane, and D. Elad, "Low jitter silicon bipolar based VCOs for applications in high speed optical communication systems," in *IEEE MTT-S Int. Microw. Symp. Dig.*, May 2001, pp. 1567–1570.

[3] Y.-T. Lee, J. Lee, and S. Nam, "High-Q active resonators using amplifiers and their applications to low phase-noise free-running and voltage-controlled oscillators," *IEEE Trans. Microw. Theory Techn.*, vol. 52, no. 11, pp. 2621–2626, Nov. 2004.

[4] P. Rice *et al.*, "A 10 GHz dielectric resonator oscillator using GaN technology," *IEEE MTT-S Int. Microw. Symp. Dig.*, Jun. 2004, pp. 1497–1500.

[5] M. Hara *et al.*, "Super-high-frequency band filters configured with air-gap-type thin-film bulk acoustic resonators," *Jpn. J. Appl. Phys*, vol. 49, no. 7, pp. 07HD13.1–07HD13.4, 2010.

[6] G. Chen and M. Rinaldi, "High-Q X band aluminum nitride combined overtone resonators," in *Proc. Joint Conf. IEEE Int. Freq. Control Symp. Eur. Freq. Time Forum (EFTF/IFC)*, Apr. 2019, pp. 1–3.

[7] M. Rinaldi, C. Zuniga, and G. Piazza, "5-10 GHz AlN contour-mode nanoelectromechanical resonators," in *Proc. IEEE 22nd Int. Conf. Micro Electro Mech. Syst.*, Jan. 2009, pp. 916–919.

[8] M. Park, Z. Hao, D. Kim, A. Clark, R. Dargis, and A. Ansari, "A 10 GHz single-crystalline scandium-doped aluminum nitride Lamb-wave resonator," in *Proc. Int. Conf. Solid-State Sensors, Actuat. Microsyst. Eurosensors XXXIII*, Jun. 2019, pp. 450–453.

[9] M. Park, J. Wang, R. Dargis, A. Clark, and A. Ansari, "Super high-frequency scandium aluminum nitride crystalline film bulk acoustic resonators," in *Proc. IEEE Int. Ultrason. Symp. (IUS)*, Oct. 2019, pp. 1689–1692.

[10] M. Ghatge, G. Walters, T. Nishida, and R. Tabrizian, "High-Q UHF and SHF bulk acoustic wave resonators with ten-nanometer $Hf_{0.5}Zr_{0.5}O_2$ ferroelectric transducer," in *Proc. 20th Int. Conf. Solid-State Sensors, Actuat. Microsyst. Eurosensors XXXIII (TRANSDUCERS EUROSENSORS XXXIII)*, Jun. 2019, pp. 450–453.

[11] D. Weinstein and S. A. Bhave, "Acoustic resonance in an independent-gate FinFET," in *Proc. Solid-State Sensors, Actuat. Microsyst. Workshop*, 2010, pp. 459–462.

[12] Y. Yang, R. Lu, T. Manzaneque, and S. Gong, "Toward Ka band acoustics: Lithium niobate asymmetrical mode piezoelectric MEMS resonators," in *Proc. IEEE Int. Freq. Control Symp. (IFCS)*, May 2018, pp. 1–5.

[13] Y. Yang, R. Lu, and S. Gong, "Scaling acoustic filters towards 5G," in *IEDM Tech. Dig.*, San Francisco, CA, USA, Dec. 2018, pp. 39.6.1–39.6.4.

[14] V. Plessky *et al.*, "Laterally excited bulk wave resonators (XBARs) based on thin lithium niobate platelet for 5 GHz and 13 GHz filters," in *IEEE MTT-S Int. Microw. Symp. Dig.*, Jun. 2019, pp. 512–515.

[15] A. Kourani and S. Gong, "A tunable low-power oscillator based on high-Q lithium niobate MEMS resonators and 65-nm CMOS," *IEEE Trans. Microw. Theory Techn.*, vol. 66, no. 12, pp. 5708–5723, Dec. 2018.

[16] A. Kourani, R. Lu, A. Gao, and S. Gong, "A 300-500 MHz tunable oscillator exploiting ten overtones in single lithium niobate resonator," in *Proc. Joint Conf. IEEE Int. Freq. Control Symp. Eur. Freq. Time Forum (EFTF/IFC)*, Apr. 2019, pp. 1–4.

[17] Y. Yang, A. Gao, R. Lu, and S. Gong, "5 GHz lithium niobate MEMS resonators with high FoM of 153," in *Proc. IEEE 30th Int. Conf. Micro Electro Mech. Syst. (MEMS)*, Jan. 2017, pp. 942–945.

[18] M. Aissi, E. Tournier, M.-A. Dubois, G. Parat, and R. Plana, "A 5.4 GHz 0.35 μm BiCMOS FBAR resonator oscillator in above-IC technology," in *IEEE Int. Solid-State Circuits Conf. (ISSCC) Dig. Tech. Papers*, Feb. 2006, pp. 1228–1235.

[19] H. Zhang, J. Kim, W. Pang, H. Yu, and E. Kim, "5 GHz low-phase-noise oscillator based on FBAR with low TCF," in *13th Int. Conf. Solid-State Sensors, Actuators Microsyst. Dig. Tech. Papers*, Jun. 2005, pp. 1100–1101.

[20] M. ElBarkouky, G. Vandersteen, P. Wambacq, and Y. Rolain, "A 7 GHz FBAR overtone-based oscillator," in *Proc. Eur. Microw. Conf.*, Sep./Oct. 2009, pp. 318–321.

[21] E. Tournier, "5.4 GHz, 0.35 μm BiCMOS FBAR-based single-ended and balanced oscillators in above-IC technology," in *MEMS-based Circuits and Systems for Wireless Communication*. New York, NY, USA: Springer, 2013, pp. 155–186.